Tellus (1994), 46A, 419–432
Printed in Belgium – all rights reserved

TELLUS
ISSN 0280–6495

Interdecadal variability in a global coupled model

By JIN-SONG VON STORCH, *Max Planck Institute for Meteorology, Bundesstrasse 55, D-20146 Hamburg, Germany*

(Manuscript received 16 August 1993; in final form 1 March 1994)

ABSTRACT

Interdecadal variations are studied in a 325-year simulation performed by a coupled atmosphere, ocean general circulation model. The patterns obtained in this study describe some of the dominant features of interdecadal variations in the model atmosphere and in the model Pacific Ocean. (1) *Atmosphere.* Interdecadal variations have no preferred time scale and can be generated by an AR(1)-process which has a longer characteristic time than that of the weather fluctuations. There are two dominant modes, one is related to variations of the tropical easterlies and the other to the Southern Hemisphere westerlies. The amplitude of the associated wind anomalies is largest in the upper troposphere. The associated temperature anomalies are in thermal-wind balance with the zonal winds and are out of phase in the troposphere and in the lower stratosphere. (2) *Pacific Ocean.* The dominant mode in the Pacific is basin-wide with a time scale of 10 to 20 years. Its signature propagates westward in the tropics and then northward (southwestward) in the North (South) Pacific. The evolution is related to changes in the upper ocean circulation and the upper ocean thermal structure. In the midlatitudes, the current changes are in Sverdrup relation with the wind changes whereas in the tropics air–sea interaction processes might be involved during a certain phase of the oscillation.

1. Introduction

Decadal time scale changes in the climate system have drawn increasing attention from researchers. For instance, Trenberth (1990) has demonstrated that there was a change in the North Pacific sea level pressure field during the winter season between 1946–76 and 1977–87. This "climate change" was seen over the North Pacific throughout the troposphere, in the North Pacific sea surface temperature (SST), and probably also in the tropical SST (see also Nitta and Yamada, 1989; Salmon, 1992; Xu, 1993). Another atmospheric circulation change was noted by Xu (1993) who found in a twenty year data set that the Southern Hemisphere westerlies became stronger after the mid-seventies. A well-known oceanic interdecadal variation is the "Great Salinity Anomaly" (GSA) which was characterized by a freshening of the surface waters of the North Atlantic during the 1960s and 1970s (Dickson et al., 1988). Interdecadal variations were also found in SST anomalies over different regions.

Some of the interdecadal variations have been studied using General Circulation Models (GCMs). The modeling studies of the oceanic variations are summarized in UNESCO (1992). For the Pacific Ocean, the modeling efforts have been mainly confined to studies using uncoupled models driven by observed boundary conditions. Both atmospheric GCMs and oceanic GCMs were successful in simulating overall features of the observed "climate change" in and over the North Pacific. However, because of the limited length of the observed boundary forcings, it is difficult to derive the basic statistics of interdecadal variations, such as time scales, from these simulations. For the atmosphere, variations on time scales longer than one year were first described by James and James (1989, 1992) in a simplified atmospheric GCM. Their principal mode could be described in terms of an alternate splitting and coalescence of the subtropical and mid-latitude jets. Although there is similarity between this mode and the Southern Hemispheric mode found in the observations (Xu, 1993), the reality of such a mode is

questionable because of the simplicity of the model and the shortness of the observational record. At this stage, the only alternative is to investigate more realistic simulations.

In this paper, the output of a long-term integration performed by a coupled GCM is used to study the interdecadal variations in the atmosphere and in the Pacific Ocean. The coupled GCM is a state-of-the-art coupled model which can be integrated over a time period of centuries. The atmospheric component of the coupled model is the ECHAM-1 T21 model which is the Hamburg version of the ECWMF operational numerical weather prediction model adapted for climate simulation purposes. The horizontal resolution is limited by a triangular spectral cut-off to a total wave number of 21 representing a 64 longitude by 32 latitude grid (Roeckner et al., 1992). The oceanic component is the Hamburg LSG (Large Scale Geostrophic) model which is based on a numerical formulation of the primitive equations for large-scale geostrophic motion. The ocean model is based on 11 variably spaced vertical levels and an effective grid-size of 4° which is coarser than the grid used by Maier-Reimer et al. (1993). Thus, the ocean component of the coupled model is a different version of that described by Maier-Reimer et al. (1993).

Before coupling, the ocean model was integrated for 7000 years in a spin-up run. The first 5000 years of this run were driven by the monthly climatological wind stress fields of Hellerman and Rosenstein (1983), and a feedback to an effective monthly mean air temperature constructed from the COADS (Woodruff et al., 1987) and the annual-mean surface salinity from Levitus (1982). The last 2000 years were driven by the fresh water fluxes which were diagnosed from the first 5000 years, and the same wind stress and air temperature forcings as used before. The final state of this integration was then coupled to the ECHAM-1 model.

The atmosphere and ocean components are coupled by the air-sea fluxes of momentum, sensible and latent heat, short and long wave radiation and fresh water (Cubasch et al., 1992). To avoid a climate drift of the coupled system, a flux correction is applied (Sausen et al., 1988) which is equivalent to coupling the atmosphere and ocean with anomalies of the fluxes computed relative to the equilibrium states of the two uncoupled sub-systems. The flux correction is designed to ensure that the climatology of the atmospheric component is essentially identical to that of the uncoupled model documented by Boer et al. (1991) and the climatology of the oceanic component is similar to that of the uncoupled ocean model. The output analyzed here contains 325 model years from year 9 to year 333. The first 100 years of the coupled-model simulation have been documented by Cubasch et al. (1992).

The state of the coupled model after 333 years of integration is briefly presented in Section 2. Two dominant atmospheric interdecadal modes are described in Section 3. In Section 4, a pronounced interdecadal mode in the Pacific is investigated. A summary is given in Section 5.

In the following, unless explicitly noted, monthly data are used for the atmosphere whereas oceanic data are yearly. In Sections 3 and 4, only anomalies are considered. They are derived by subtracting the 325-year mean annual cycle for the atmospheric data and by subtracting the 325-year annual-mean for the oceanic data.

2. The State of the coupled model

Before analyzing the variability, we summarize a few salient features of the coupled model. The mean fields are averaged over 325 years. Figs. 1a, b show the zonally-averaged profiles of the zonal wind component in January and July. The amplitude and the location of the major tropospheric jets are simulated reasonably well, but the secondary wind maximum of the Southern Hemisphere winter-time double-jet is too weak, a feature typical of low resolution models (Xu et al., 1990). The largest variances of the zonal mean zonal wind anomalies are located over the high latitudes and in the upper troposphere (Fig. 1c).

The 325-year mean and standard deviation of the vertically integrated oceanic mass transport streamfunction are shown in Fig. 2. The structure and intensity of the circulation are similar to those produced by the uncoupled model, except for a stronger subpolar gyre in the North Atlantic (Maier-Reimer et al., 1993). The variance maxima in the southern oceans indicate variations of the Antarctic Circumpolar Current of order of 5 Sv. In the North Pacific and North Atlantic, variance maxima of order of 2 Sv are situated in the centers of the oceans.

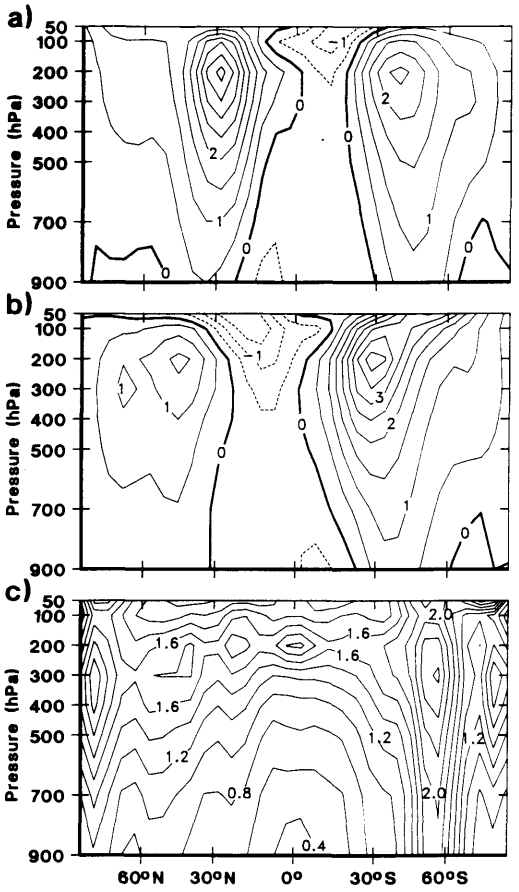

Fig. 1. 325-year average of January (a) and July (b) zonal mean zonal wind profiles (10 ms^{-1}) and standard deviation of the monthly zonal mean zonal wind anomalies (c) (ms^{-1}).

The mean state of the zonally averaged meridional overturning circulation (streamfunction) in the Atlantic is shown in Fig. 3. This parameter is only defined north of 30° S where the meridional boundaries end. The characteristic features of the overturning are an inflow of order of 10 Sv from the Southern Ocean in the upper kilometer, a strong outflow of order of 20 Sv from the North Atlantic, and a small bottom inflow from the south. The bottom inflow is weaker in the coupled model than in the uncoupled model (Fig. 3b from Maier-Reimer et al., 1993).

Fig. 4 shows time series of globally averaged 500-mb temperature, ice thickness and 2000-meter ocean temperature. The atmosphere is quasi-stationary with respect to the global mean 500-mb temperature. A comparison between the time series of 500-mb temperature and ice thickness suggests that the decrease (increase) of the tropospheric temperature in the first 80 (afterward) years is related to the growth (decay) of the global ice volume. The magnitude of the ice-related temperature changes is about 0.5 K.

In contrast to the atmosphere, the ocean is not yet in equilibrium. There is a global warming of about 0.1 to 0.2 K per 300 years in the model ocean. The warming comes to an end in the upper ocean after 100 years. In the Pacific for instance, the surface of $\rho = 26.6\ kg\ m^{-3}$ rises 40 m within the first 100 years and then stays quasi-stationary. At the 4000-m depth, however, the temperature increases throughout the integration without any indication of reaching a nearby stationary state.

3. Interdecadal modes in the atmosphere

3.1. Temporal and spatial structures

To study the temporal features of the interdecadal atmospheric variations, we first consider spectra which are obtained by averaging those of the time series at each grid point. The top curve in Fig. 5 is such an averaged spectrum for the local 200-mb streamfunction. It consists of two parts: one for time scales shorter than 2 years which is derived from 10 years of daily anomalies (model years 91 to 100); and one for time scales longer than 2 months which is derived from 325 years of monthly anomalies. At the overlapping frequencies, the two spectra have the same energy level.

In general, there is an increase of energy with increasing time scale. The spectrum is red and shows a wide plateau without any pronounced spectral peak on the time scale longer than one year. The spectral maximum at the low-frequency end is related to the trend of the time series (see Fig. 7). The model atmosphere does not prefer any specific frequency on time scales longer than 1 year in terms of averaged spectra.

Since the interdecadal variations might be related to specific spatial patterns, several EOF and POP (see Section 4) analyses were carried out to study the spatial structure of variations on time scales longer than 1 year. The dominant modes have the character of standing signals and can be described by the leading EOFs. Fig. 6 shows

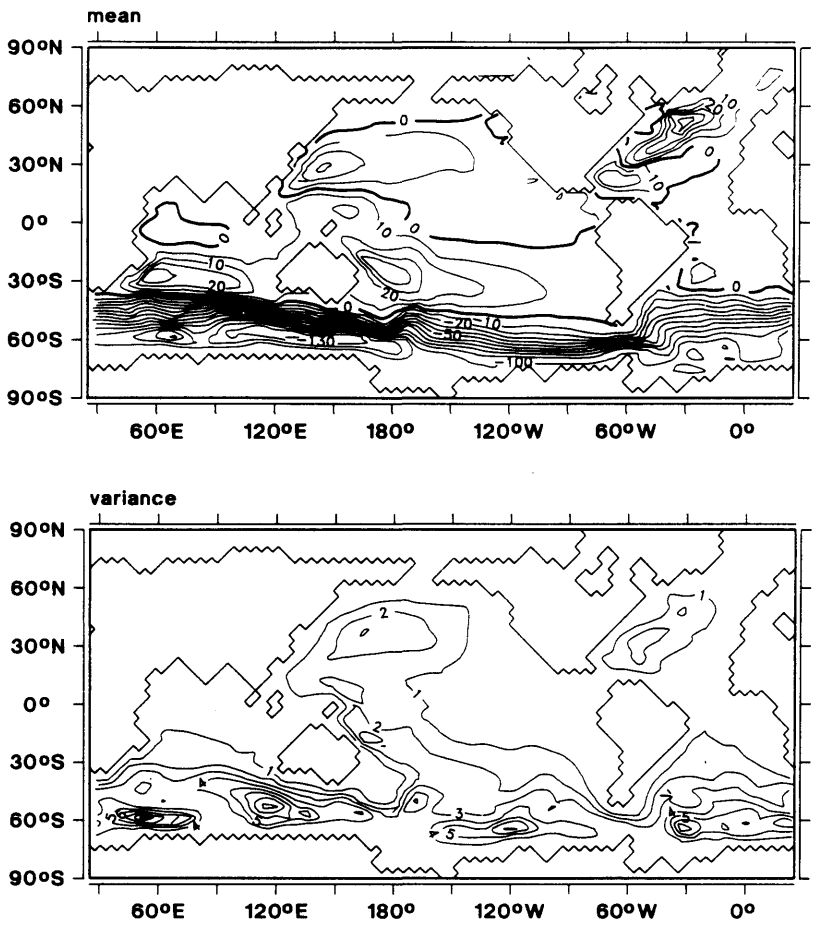

Fig. 2. 325-year average of vertically integrated annual-mean mass transport streamfunction (top) and standard deviation of the yearly streamfunction anomalies (bottom). Both in Sv.

EOF1 and EOF2 obtained from filtered 200-mb streamfunction where variations on time scales shorter than 7 years and longer than 50 are suppressed. They explain together 63% of the filtered variance. The patterns change very little when different filter windows are used or streamfunctions at different levels are chosen (not shown), which suggests that EOF1 and EOF2 are the dominant patterns (in terms of variance) of the atmospheric variations on time scales longer than 1 year.

The coefficient time series of EOF1 and EOF2 are obtained by projecting the monthly or daily (only years 91 to 100) unfiltered 200-mb streamfunction data onto EOF1 and EOF2 (Fig. 6). Yearly values of these coefficients are shown in Fig. 7. The spectra of PC1 and PC2 (the lower two in Fig. 5) are redder than the averaged spectrum (the top one in Fig. 5). Where does the redness come from? In the case when only short time scale weather fluctuations exist, such variability would generate variance on interdecadal time scales. As in the concept of potential predictability (Madden, 1976), we have to discriminate between that part of the interdecadal variations that stems from the weather noise and that part which reflects other (unknown) slower processes.

To answer this question, first-order autoregressive (AR(1)) processes are fitted to both the daily and monthly PC time series and the daily anomalies of the 200-mb streamfunction at each

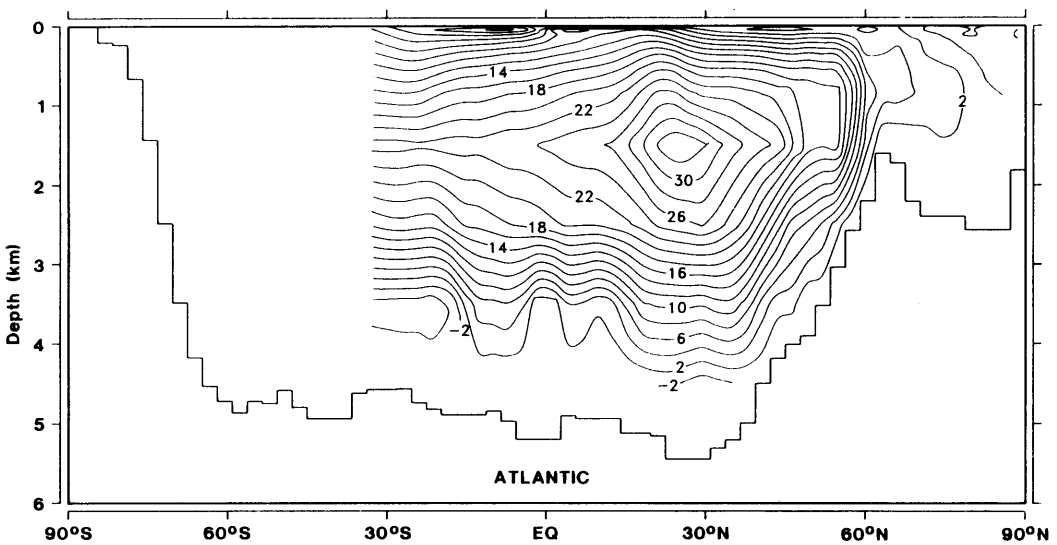

Fig. 3. 325-year average of the zonally integrated meridional streamfunction in the Atlantic (Sv).

grid point, and decorrelation times $(1+\gamma)/(1-\gamma)$, with γ being the coefficient of an AR(1)-process, are calculated. It turns out that the spectra of the PC time series (the two lower ones in Fig. 5) and of the local time series (the top one in Fig. 5) can be well reproduced by the fitted AR(1)-spectra. However, the decorrelation time of both monthly and daily PC time series is about 2 to 3 months whereas the decorrelation time averaged over all grid points is about 10 days. Since weather fluctuations have small spatial scales, their characteristic times can be approximated by those of grid-point time series. The results suggest that EOF1 and EOF2 are generated by an AR(1)-process which has a much longer characteristic time than that of the weather fluctuations. Thus, PC1 and PC2 do

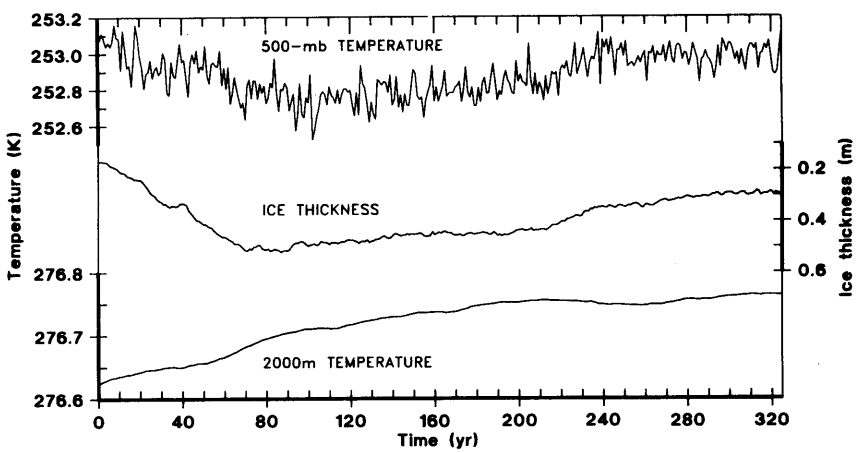

Fig. 4. Time series of globally averaged 500-mb temperature (K), ice-thickness (m) and 2000-meter temperature (K). Note that the global average of the ice thickness does not correspond to the mean ice thickness since ice is not a global variable.

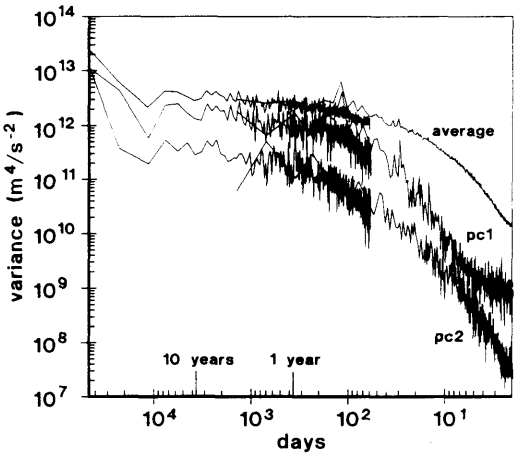

Fig. 5. Spectra of 200-mb streamfunction and of PC1 and PC2. All three spectra are derived from averaging those of the time series at each grid point, the top one corresponds to the unfiltered 200-mb streamfunction fields and the other two correspond to fields which are reproduced by multiplying EOF1 (EOF2) by PC1 (PC2).

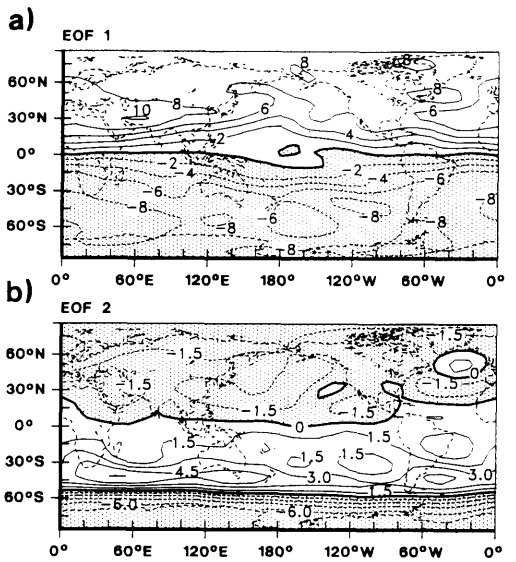

Fig. 6. EOF1 and EOF2 calculated from 200-mb streamfunction anomalies. The data are filtered in such a way that variations on time scales shorter than 7 years and longer than 50 years are suppressed.

not merely integrate the action of the local weather noise.

Back to the spatial structures, Fig. 8 shows patterns of zonal mean zonal wind and zonal mean temperature which are related to PC1 and PC2. They are called regression patterns and are calculated by minimizing the following equation:

$$\left\langle \left(x(t) - \frac{\alpha(t)}{\delta} p \right)^2 \right\rangle = \min, \qquad (1)$$

where $\langle\ \rangle$ indicates expectation, $\alpha(t)$ is PC1 or PC2, δ its standard deviation, and $x(t)$ anomalies of zonal mean zonal wind or zonal mean temperature. As the solution of (1), the regression p_i at the ith grid point is simply the correlation between the normalized PC and x_i. The normalization ensures that the values in a regression pattern correspond to one-standard-deviation anomalies in physical units.

Compared with the mean state (Fig. 1), EOF1 is associated with changes in the intensity of the

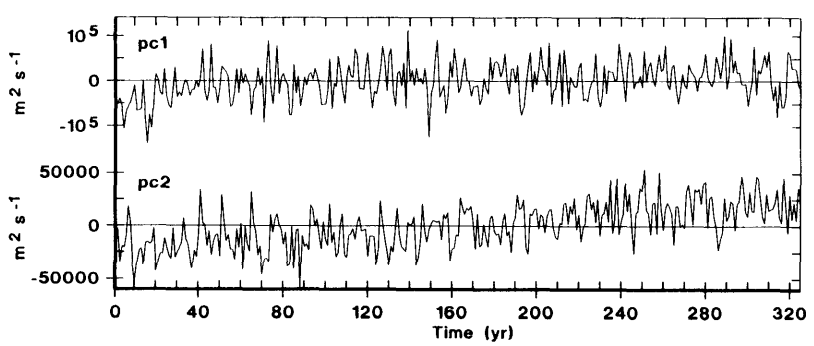

Fig. 7. PC1 and PC2 in $m^2\,s^{-1}$. They are derived by projecting the unfiltered monthly anomalies onto normalized EOF1 and EOF2 and then taking an average for each year.

tropical easterlies (Fig. 8a) and EOF2 with a shift of the Southern Hemispheric jet (Fig. 8b). The wind anomalies are in thermal wind balance with the temperature anomalies. Since the winds have their largest amplitude in the upper troposphere, the meridional temperature gradient changes its sign around the tropopause so that the temperature anomalies in the troposphere are out of phase with those in the lower stratosphere (Fig. 8c, d). In the tropics (over the Southern Ocean), Fig. 8a (b) explains up to 60% of the total unfiltered variance of the zonal mean zonal winds whereas Fig. 8c (d) up to 20 to 30% of the total unfiltered variance of the zonal mean temperature. The one-standard-deviation wind anomalies are of order of 1 to 1.5 ms^{-1} and those of temperature, 0.2 to 0.5 K. The amplitude of the temperature anomalies is comparable to the largest variability in the tropospheric temperature changes which are related to the ice variations (Fig. 4).

The Southern Hemispheric tripole-structure in Fig. 8b has larger meridional and vertical scales than the mode found in the simplified model of James and James (1992).

3.2. *The role of the ocean*

To study the possible role of the ocean in generating the atmospheric modes described in Subsection 3.1, sensible and latent heat flux anomalies are considered. Apart from radiation, the heat fluxes through the air-sea interface are the only external forcing for the atmosphere, insofar as they depend on external parameters such as SST and sea ice skin temperature.

Two conceptually opposite cases are considered. In the case when atmospheric variations are not generated by the underlying oceans, the heat flux forcing $f(t)$ would vary in phase with the PC time series $\alpha(t)$:

$$\alpha(t) \sim f(t). \tag{2}$$

It is assumed that the heat flux forcing displays the same spatial structure on all time scales and

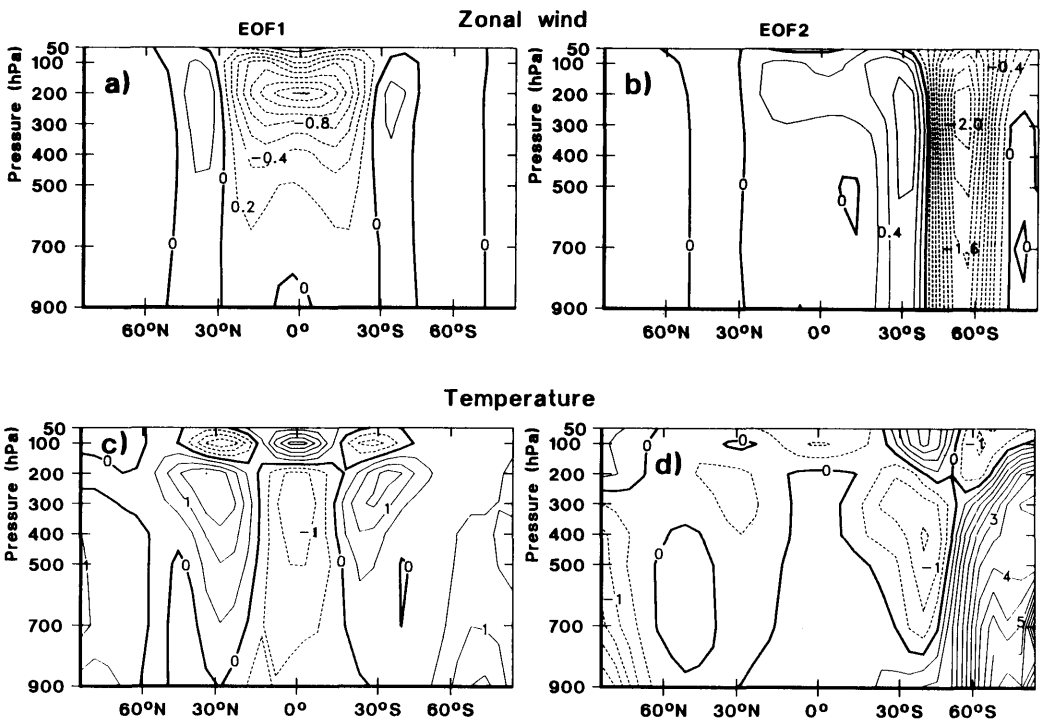

Fig. 8. Regression patterns of anomalies of zonal mean zonal winds (ms^{-1}, top) and zonal mean temperature (0.1 K, bottom) related to EOF1 (left) and EOF2 (right).

that its temporal evolution is given by $f(t)$. This assumption is reasonable because the atmospheric variations which are given by Figs. 6, 8 have the same structures on different time scales. If eq. (2) holds, the anomalous atmospheric circulation would produce changes in the wind driven circulation of the ocean which would develop parallel to PC1 and PC2.

Eq. (2) would also be true if a tropical air–sea interaction process is involved. In this case, wind anomalies would develop parallel to tropical SST anomalies.

If the atmospheric variations were entirely generated by the underlying oceans, the corresponding heat flux forcing $f(t)$ would be 90° out of phase with $\alpha(t)$ over a wide frequency band and satisfy:

$$\frac{d\alpha(t)}{dt} \sim f(t). \tag{3}$$

The two proposed relations (2) and (3) are tested by calculating the regression patterns between $\alpha(t)$ and heat flux and between $d\alpha(t)/dt$ and heat flux. The largest signal is found in the in-phase relationship whose patterns explain up to 5% of the total variance in the tropical region for latent heat flux and up to 10% in the southern oceans for sensible heat flux. The 90° out of phase relationship which is shown by the regression

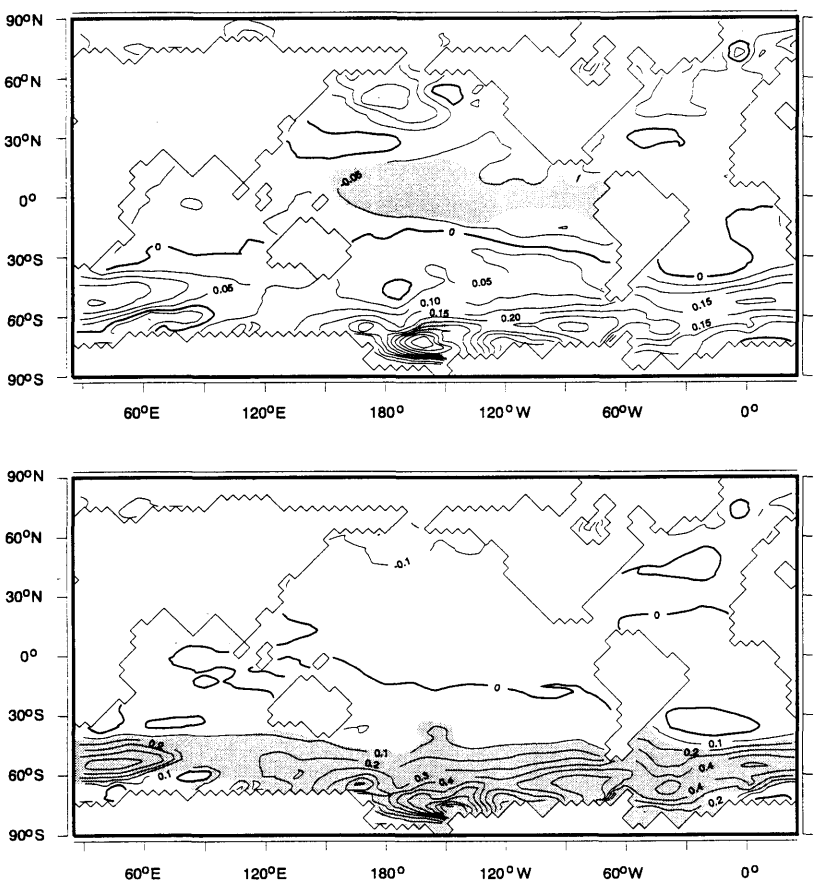

Fig. 9. Regression patterns of anomalies of sea surface temperature anomalies (K) related to EOF1 (top) and EOF2 (bottom). The shaded areas indicate regions where the variance explained by the corresponding regression pattern is larger than 10%.

patterns between heat flux and $d\alpha(t)/dt$ have patchy structures and explain no variance at all. A direct forcing-response relation between heat flux and out modes cannot be found in the form of (3).

The regression patterns for SST are shown in Fig. 9 where shaded areas indicate areas where explained variance is larger than 10%. The EOF1 related negative SST anomalies in the tropics (the top diagram of Fig. 9) appear together with well organized easterly wind stress anomalies and anomalous upwelling in the tropics (not shown). The EOF2 related positive SST anomalies in the Southern Ocean (the bottom diagram of Fig. 9) appear together with easterly wind stress anomalies over the Southern Ocean which cause weaker Antarctic Circumpolar Current, and an anomalous southward Ekman transport and anomalous downwelling north of the Antarctic (not shown). These in phase relationships suggest that EOF1 and EOF2 are either atmospheric modes or, in case of EOF1, a result of tropical air–sea interactions.

4. An interdecadal mode in the Pacific Ocean

In contrast to the atmosphere, Pacific interdecadal variations display propagating features on time scales of about 10 to 20 years. The Principal Oscillation Pattern (POP) analysis (Hasselmann, 1988; Von Storch et al., 1988) is applied to the Pacific sea level data in order to identify the temporal and spatial characteristics of these variations. Because of the trend in temperature and salinity (Section 2) which is also reflected in the surface elevation, only filtered sea level time series are used where variability on time scales shorter than 4 years and longer than 60 years is suppressed. The same filter is applied to all other parameters which are considered in this section.

The POP analysis assumes that the multivariate time series can be described by a first-order multivariate autoregressive process. The system matrix A of this process is estimated from the lag-1 and lag-0 covariance matrix of the considered time series. The eigenvalue of A indicates the frequency with which the corresponding eigenvectors (which are called POPs) oscillate. In the case of complex POPs, the coefficient time series of the real and imaginary part of the eigenvector are 90° out of phase and oscillate coherently with the frequency given by the eigenvalue. The corresponding POP patterns follow each other on time intervals of about one quarter of a period and describe the spatial evolution of the signal.

4.1. Temporal and spatial structure

One dominant mode which appears as a complex POP is found in the Pacific sea level. Fig. 10 shows the coefficient time series. The dashed line in Fig. 10 leads the solid line by about 90°. This implies that the pattern associated with the dashed line (Fig. 11a) appears about a quarter of an oscillation period earlier than that associated with the solid line (Fig. 11b). The oscillation period, as derived from the POP analysis, is 17 years. The mode, as monitored by the POP coefficient time series (Fig. 10), is more intense in the model years from 70 to 100 and around model years 190 and 310.

The first POP pattern (Fig. 11a) is characterized by positive sea level anomalies in the tropical central and eastern Pacific and negative anomalies northwest and southwest of these. After a quarter of a period, the tropical anomalies have moved

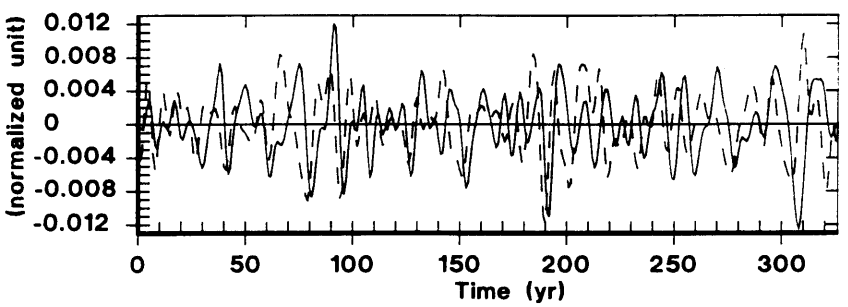

Fig. 10. Real and imaginary part of the complex coefficient time series of the Pacific mode as derived from a POP analysis for sea level anomalies.

westward and appear more pronounced north of the Equator (Fig. 11b), while negative anomalies have propagated northward in the North Pacific and southwestward in the South Pacific. The time interval which is needed for anomalies to occur and to cross the subtropical Pacific is about 4 to 5 years.

Amplitudes of the associated sea level anomalies can be derived by multiplying the POP patterns (Fig. 11) by their coefficient time series (Fig. 10) which gives sea level anomalies of about 0.5 to 1 cm. The Pacific mode explains up to 35% of the total filtered variance. The northern part of the mode is more pronounced than the southern part.

The Pacific mode is reflected not only in sea level but also in other parameters. The 3-dimensional structure is again studied by means of regression patterns. In this case, the equation to be minimized is:

$$\left\langle \left(\boldsymbol{x}(t) - \frac{z_r(t)}{\delta_r}\boldsymbol{p}_r - \frac{z_i(t)}{\delta_i}\boldsymbol{p}_i \right)^2 \right\rangle = \min, \qquad (4)$$

where $\boldsymbol{x}(t)$ is anomalies of the considered parameter, $z_r(t)$ and $z_i(t)$ are the coefficient time series of the real and imaginary part of the complex POP with standard deviations denoted by δ_r and δ_i (Fig. 10), and $\boldsymbol{p}_r$ and $\boldsymbol{p}_i$ the regression patterns of this parameter. The parameters are filtered in the

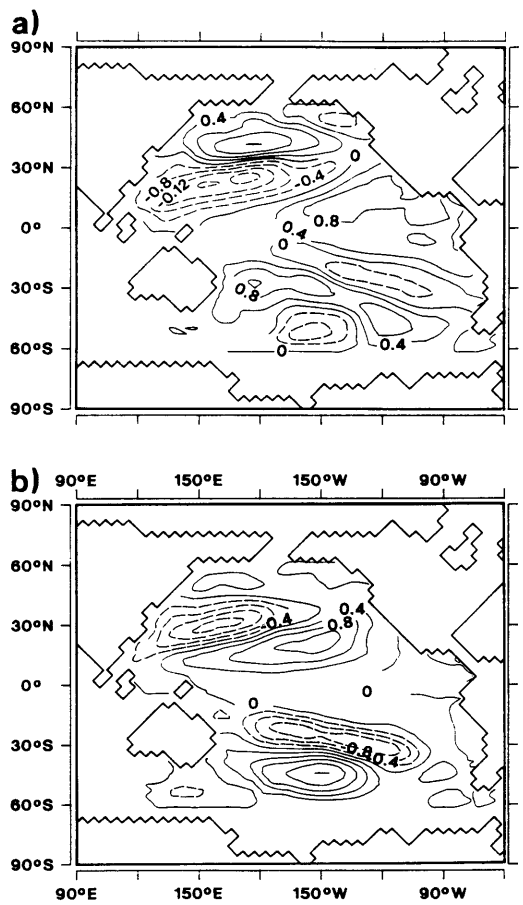

Fig. 11. Characteristic patterns of the Pacific mode as derived from a POP analysis for sea level anomalies. The upper diagram appears about one quarter of a period earlier than the lower diagram.

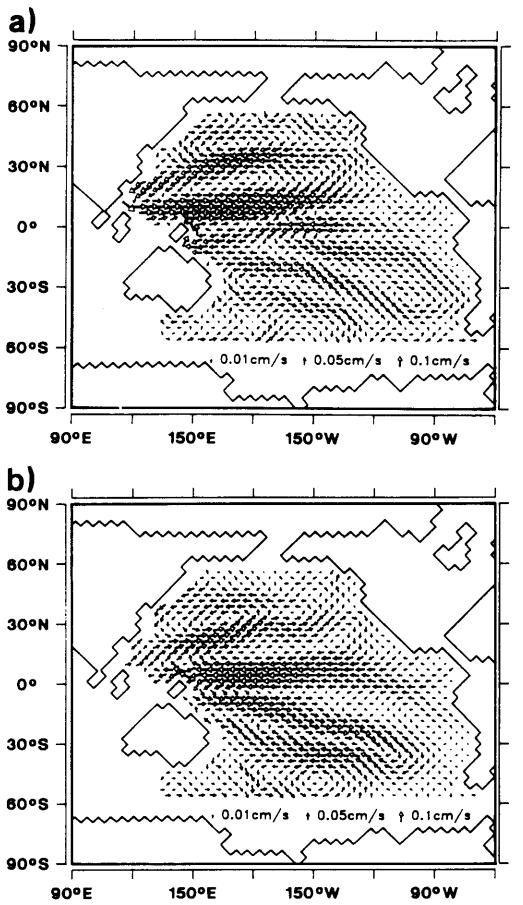

Fig. 12. Characteristic patterns of the Pacific mode found in 150-meter velocity (cm/s). They have the same temporary evolution as those indicated by the POP coefficient time series.

same way as for sea level, that is, variability on time scales shorter than 4 years and longer than 60 years is suppressed. The regression patterns and POP patterns display the same temporal evolution as that indicated by the POP coefficient time series and give a complex description of the mode.

According to the regression patterns, the Pacific mode is related to changes of the current and of the thermal structure. In the upper ocean, the current changes are in geostrophic balance with the sea level anomalies. Fig. 12 shows the patterns of 150-meter current anomalies.

The changes in the vertical thermal structure are shown by regression patterns of temperature anomalies in a vertical cross-section along about 15°N (Fig. 13). The positive (negative) sea level anomalies in the subtropical eastern (western) Pacific (Fig. 11a) are accomplished by sinking (lifting) of isotherms in the same region (Fig. 13a). After a quarter of a period, the isotherms deepen in the upper few hundred meters across almost the entire Pacific along 15°N (Fig. 13b) as the positive sea level anomalies move into the central Pacific in Fig. 11b. Thus, parallel to the evolution of the sea level anomalies, temperature anomalies also move westward with the largest anomalies being located at 150 to 250 meters depth in the west and at 75 to 150 meters in the east which corresponds to the upper part of the model thermocline.

The vertical structure of the temperature anomalies and the time interval which is needed for sea level anomalies to cross the subtropical Pacific suggest the active role of the first baroclinic Rossby waves in the evolution of the Pacific mode. The unusual part of the evolution, however, is the subsequent northward (southwestward) propagation in the North (South) Pacific.

4.2. *The atmospheric forcing*

Regression patterns have been calculated for wind stress, heat flux and freshwater flux. Atmospheric anomalies are averaged for each year since only yearly sea level data are used.

Fig. 14 shows regression patterns for zonal wind

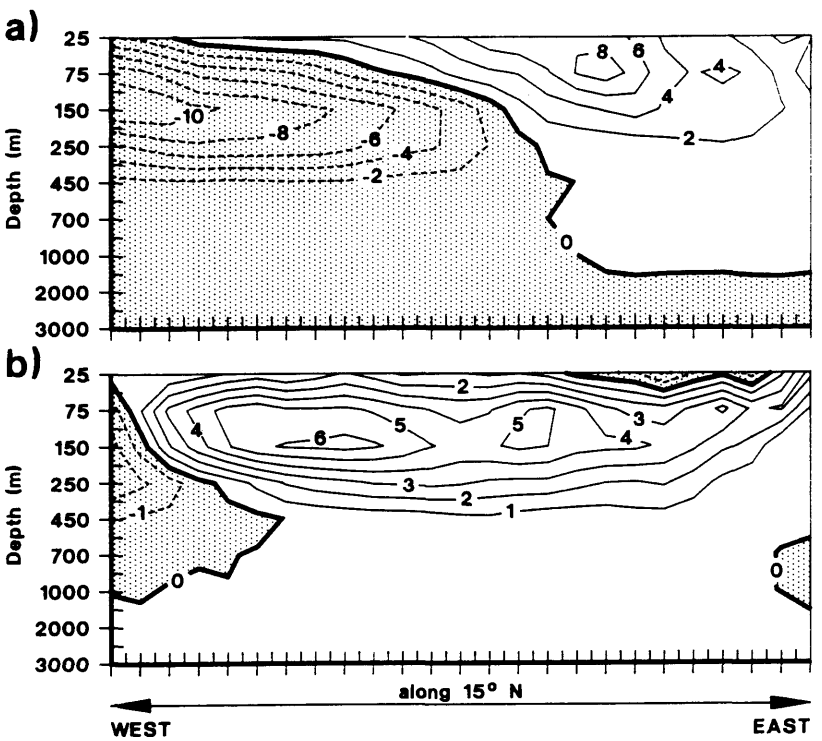

Fig. 13. Characteristic temperature patterns of the Pacific mode found in a longitude-height cross-section along 15°N (10^{-2} K). They have the same temporary evolution as those indicated by the POP coefficient time series.

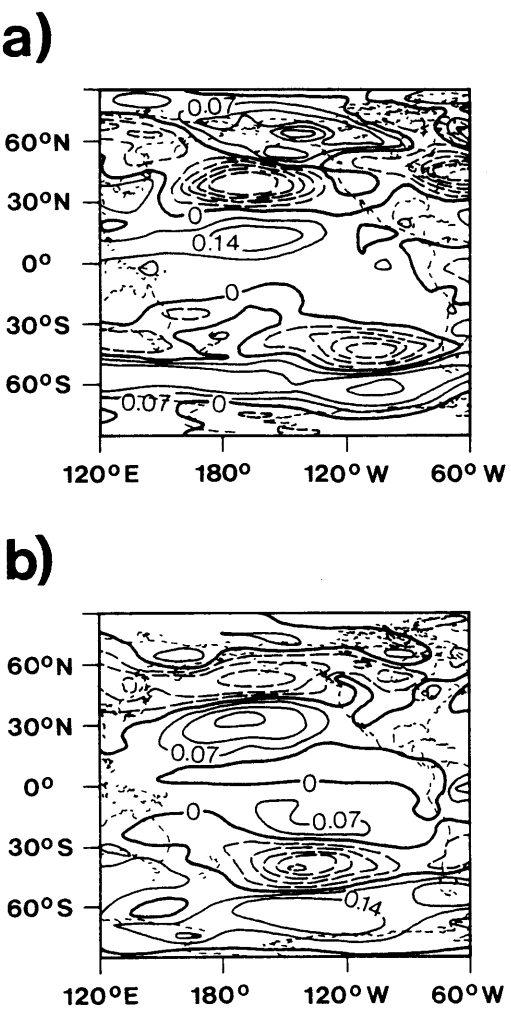

Fig. 14. Zonal wind stress patterns which are related to the Pacific mode. They have the same temporary evolution as those indicated by the POP coefficient time series (Pa).

stress. In the midlatitudes, anomalies of the zonal wind stress (Fig. 14) and the current (Fig. 12) are in Sverdrup relation, that is, the maxima of the positive (negative) wind stress curl coincide with northward (southward) current anomalies. Towards the tropics, the relationship between the wind stress and the current is only notable in one stage of the cyclic evolution of the Pacific mode, namely the stage described by Fig. 12a where the eastward current anomalies along about 15°N are associated with westerly anomalies over the same area in Fig. 14a. In the other stage which appears after a quarter of a period (Fig. 12b), the large anomalous westward current in the tropical Pacific is accompanied by very weak wind anomalies.

Regression patterns for the heat flux anomalies suggest that there is an exchange of heat flux between the atmosphere and the ocean in the tropical and the North Pacific regions (not shown), especially during the stage described by Fig. 11a, 12a and 13a. During this stage, positive SST anomalies in the central and eastern tropical Pacific (not shown) appear together with the westerly wind stress anomalies in the tropical Pacific (Fig. 14a). These SST might induce changes in large-scale tropical convection which in turn produces changes in the SST. The result suggests that tropical air–sea interaction processes might be involved at this stage of the oscillation.

The wind stress changes (Fig. 14) and the related changes in the Aleutian Low (not shown) resemble the changes observed during the mid-seventies. This paper suggests that the observed patterns are part of a more complete oscillatory phenomenon of the whole Pacific Ocean which is related to variations in the wind-driven circulation and the oceanic thermal structure.

5. Conclusions

Characteristics of atmospheric and Pacific inter-decadal variability in a 325-year simulation with the Hamburg ECHAM/LSG model are identified. There are two dominant atmospheric modes in the model, one in the tropics and the other in the Southern Hemisphere. Both display the following characteristic features:

- *No preferred time scale.* The spectra of the corresponding time series are red.
- *Zonal scale.* The structure has zonal wave number zero.
- *Vertical scale.* Features extend throughout the atmosphere with largest anomalies in the upper troposphere.
- *Temperature structure.* The troposphere is out of phase with the lower stratosphere.
- *Amplitude.* Typical magnitude for zonal mean zonal wind is about 1–1.5 ms^{-1}, and for zonally averaged temperature about 0.2 K.

• *The role of the ocean.* For EOF1, the in phase relationship between the tropical wind and SST anomalies indicates that tropical air–sea interaction processes might be involved. For EOF2, the oceanic anomalies are found to be wind driven. The passive role of the ocean in generating EOF2 is consistent with the results of James and James (1992) who used a simplified atmospheric model without an oceanic component.

The coupled model generates a dominant interdecadal mode in the Pacific Ocean with the following features:

• *Oscillation period of about 17 years.* The intensity of the oscillation, however, varies irregularly.

• *Spatial and vertical scales.* The horizontal scale of the Pacific mode is basinwide. In the vertical direction, temperature anomalies have their largest values in the upper model thermocline and vanish in the deep ocean.

• *Propagation within the basin.* The Pacific mode appears to circulate within the North and South Pacific with the movement of anomalies westward in the tropics, northward in the North Pacific, and southwestward in the South Pacific.

• *Atmospheric forcings.* In the midlatitude regions, wind stress forcings and the current anomalies are in Sverdrup relation; whereas in the tropics, air–sea interaction processes may play an active role during a certain phase of the oscillation.

The 325-year simulation of the coupled ECHAM1/LSG model enables us to study the dominant temporal and spatial characteristics of the interdecadal climate variations. The long-term atmospheric variations reveal well-organized structures. Their spectra can be reproduced by AR(1)-spectra with characteristic time of about 2 to 3 months. This suggests that the interdecadal atmospheric variability results from the integration of an unknown process which has longer time scales than the weather fluctuations. In the Pacific Ocean, the dominant mode has a time scale of order of 10 to 20 years which is related to the propagation and evolution of anomalies of temperature and currents within the Pacific Ocean.

This paper is a first description of the low-frequency variations generated by our coupled GCM. Further detailed analyses are needed to investigate the origin of these variations.

6. Acknowledgments

I express my gratitude to Ulrich Cubasch, Eduardo Zorita, Gabi Hegerl and Dierk Schriever who supported me with the coupled model simulations. Thanks to Claude Frankignoul for his valuable comments as reviewer, and to Ernst Maier-Reimer and Hans von Storch for their help in diagnosing the state of the model ocean and in formulating the results, and to Peter Müller and Gary Mitchum for interesting discussions during my stay in their institute. Thanks also to Heinke Höck for assisting me with ocean model post processing, Reiner Schnur, Gabi Hegerl and Peter Wright for helping me with the English and Marion Grunnert for preparing the diagrams.

REFERENCES

Boer, G. J., Arpe, K., Blackburn, M., Deque, M., Gates, W. L., Hart, T. L., Le Treut, H., Roeckner, E., Sheinin, D. A., Simmonds, I., Smith, R. N. B., Tokioka, T., Wetherald, R. T. and Williamson, D. 1991. *An intercomparison of the climates simulated by 14 atmospheric general circulation models.* WMO/TD-No. 425, Geneva, Switzerland.

Cubasch, U., Hasselmann, K., Höck, H., Maier-Reimer, E., Mikolajewicz, U., Santer, B. D. and Sausen, R. 1992. Time-dependent greenhouse warming computations with a coupled ocean-atmosphere model. *Climate Dyn.* **8**, 55–69.

Dickson, R. R., Meincke, J., Malmberg, S. A. and Lee, A. J. 1988. The "Great Salinity Anomaly" in the northern North Atlantic 1968–1982. *Prog. Oceanogr.* **20**, 103–151.

Hasselmann, K. 1988. PIPs and POPs: The reduction of complex dynamical systems using principal interaction and oscillation patterns. *J. Geophys. Res.* **93**, 11015–11021.

Hellerman, S. and Rosenstein, M. 1983. Normal monthly wind stress over the World Ocean with error estimates. *J. Pys. Oneanogr.* **13**, 1093–1104.

James, I. N. and James, P. M. 1989. Ultra-low-frequency variability in a simple atmospheric circulation model. *Nature* **342**, 53–55.

James, I. N. and James, P. M. 1992. Spatial structure of ultra-low-frequency variability of the flow in a simple

atmospheric circulation model. *Q. J. Roy. Met. Soc.* **118**, 1211–1233.

Levitus, S. 1982. Climatology atlas of the world ocean. *NOAA Professional Paper 13*, 173 pp.

Madden, R. A. 1976. Estimates of the natural variability of time averaged sea level pressure. *Mon. Wea. Rew.* **104**, 942–952.

Maier-Reimer, E., Mikolajewicz, U. and Hasselmann, K. 1993. Mean circulation of the Hamburg LSG OGCM and its sensitivity to the thermohaline surface forcing. *J. Phys. Ocean.* **23**, 731–757.

Nitta, T. and Yamada, S. 1989. Recent warming of tropical sea surface temperature and its relationship to the Northern Hemisphere circulation. *J. Met. Soc. Japan* **67**, 375–383.

Roeckner, E., Arpe, K., Bengsson, L., Brinkop, S., Duemenil, L., Esch, M., Kirk, E., Lunkeit, F., Ponater, M., Rockel, B., Sausen, R., Schlese, U., Schubert, S. and Windelband, M. 1992. *Simulation of the present-day climate with the ECHAM model: impact of model physics and resolution.* Report 93, Max-Planck Institut fuer Meteorology, Hamburg, Germany.

Salmon, D. 1992. *On interannual variability and climate change in the North Pacific.* PhD. thesis, University of Alaska.

Sausen, R., Barthel, K. and Hasselmann, K. 1988. Coupled ocean-atmosphere models with flux corrections. *Clim. Dyn.* **2**, 154–163.

Trenberth, K. E. 1990. Recent observed interdecadal climate changes in the Northern Hemisphere. *Bull. Am. Meteor.* **71**, 988–993.

UNESCO, 1992. *Oceanic interdecadal climate variability.* IOC Technical series 40, 7, Place de Fontenoy, 75352 Paris 07 SP.

Von Storch, H., Burns, T., Fischer-Bruns, I. and Hasselmann, K. 1988. Principal oscillation pattern analysis of the 30 to 60 day oscillation in a GCM. *J. Geophys. Res.* **93**, 11022–11036.

Weisse, R., Mikolajewicz, U. and Maier-Reimer, E. 1994. Decadal variability of the North Atlantic in an ocean general circulation model. *J. Geophys. Res.*, in press.

Woodruff, S., Slutz, R. J., Jenne, R. L. and Steurer, P. M. 1987. A comprehensive ocean-atmosphere dataset. *Bull. Amer. Meteor. Soc.* **68**, 1239–1250.

Xu, J. S., Von Storch, H. and Van Loon, H. 1990. The performance of four spectral GCMs in the Southern Hemisphere: the January and July climatology and the semiannual wave. *J. Climate* **3**, 53–70.

Xu, J. S. 1993. The joint modes of the coupled atmosphere-ocean system observed from 1967 to 1986. *J. Climate* **6**, 816–838.